Adherent-suspension plasticity promotes the dissemination and colonization of circulating tumor cells

Hyunbin D. Huh[1]†, Yujin Sub[2]†, Jee Hung Kim[3,4], Hannah Lee[1], Jongwook Oh[2], Dong Ki Lee[3], Jong Hwa Byun [1], Woo Yang Pyun[1], Soong June Bae[3,4], Sehyung Pak[5], Hai-Chon Lee[5], Yu Suk Choi[6], Junjeong Choi[7], Joon Jeong[3,4]*, Heon Yung Gee[2,8]*, and Hyun Woo Park[1]*

[1] Department of Biochemistry, College of Life Science and Biotechnology, Brain Korea 21 Project, Yonsei University; Seoul 03722, Republic of Korea.

[2] Department of Pharmacology, Graduate School of Medical Science, Brain Korea 21 Project, Yonsei University College of Medicine; Seoul 03722, Republic of Korea.

[3] Division of Medical Oncology, Department of Internal Medicine, Gangnam Severance Hospital, Yonsei University College of Medicine, Seoul, Korea.

[4] Institute for Breast Cancer Precision Medicine, Yonsei University College of Medicine, Seoul, Republic of Korea.

[5] CytoGen, Inc., Seoul, Republic of Korea

[6] School of Human Sciences, University of Western Australia; Crawley, WA, 6009, Australia

[7] College of Pharmacy, Yonsei Institute of Pharmaceutical Sciences, Yonsei University, Incheon, Republic of Korea.

[8] Woo Choo Lee Institute for Precision Drug Development

† Equal contributions

*Corresponding authors. Email: Hyun Woo Park (hwp003@yonsei.ac.kr), Heon Yung Gee (hygee@yuhs.ac), Joon Jeong (gsjjoon@yuhs.ac)

Abstract

Background

The adherent-to-suspension transition (AST) describes how solid tumor cells reprograms their anchorage dependency via defined hematopoietic transcriptional regulators to disseminate into circulating tumor cells (CTCs). It remains unclear, however, whether the dissemination and colonization processes require dynamic plasticity of AST factor expression in CTCs to permit the completion of the metastatic cascade.

Methods

We investigated AST factor-mediated adherent-suspension plasticity (ASP) in a newly developed cell-based dissemination assay. Here we identified a rare population of CTC-like cells spontaneously suspended from highly confluent breast cancer cells under chronic stress conditions that mimic the tumor microenvironment (TME). We investigated the oscillatory dynamics of AST factor expression in these CTC-like cells and their role in dissemination and colonization. Furthermore, we performed a single-cell transcriptomic analysis of matched primary tumors, CTCs, and metastatic lesions from newly enrolled *de novo* metastatic breast cancer patients, focusing on the plasticity of AST factor expression during the metastatic cascade *in vivo*.

Results

Using data obtained from the dissemination assay and *de novo* metastatic breast cancer patients, we have demonstrated the dynamic regulation of AST factor expression during the dissemination and colonization of CTCs both *in vitro* and *in vivo*. From our dissemination assay of breast cancer cell lines, we show that AST factor induction is required for the reprogramming of anchorage dependency and spontaneous detachment of CTC-like cells. We also show that subsequent AST

49 factor suppression is required for the reattachment of CTCs during colonization. Single-cell
50 transcriptome analyses in matched specimens of primary tumor, CTC, and metastatic lesions
51 obtained from *de novo* metastatic breast cancer patients confirmed the oscillatory dynamics of
52 AST factors and related gene signatures related to the adherent-suspension plasticity.

53 **Conclusion**

54 Our results show that the reprogramming of anchorage dependency in solid tumor cells via AST
55 factor-mediated ASP plays a critical role in the dissemination and colonization of CTCs. These
56 findings highlight the potential of targeting AST factors to develop effective anti-metastatic
57 therapies.

Introduction

Metastasis continues to pose significant challenges in cancer treatment and remains the leading cause of cancer-related deaths. Metastatic dissemination of primary tumor cells requires the detachment of circulating tumor cells (CTCs) into the lymphatic or blood microvasculature, resist anoikis while migrating through the bloodstream, and adapt to foreign microenvironment in distant tissues [1, 2]. The metastatic cascade, therefore, could be perceived as a consequence of cancer cells constantly transitioning between an adherent state and a suspension state [3]. We recently discovered a biological phenomenon, adherent-to-suspension transition (AST), a mechanism that reprograms the anchorage dependency of solid tumor cells via hematopoietic transcription factors termed AST factors to facilitate the dissemination and release of circulating tumor cells (CTCs) [4-7]. Despite the absence of lineage differentiation and EMT (epithelial-to-mesenchymal transition), the induction of AST in solid tumor cells 1) suppresses global integrin/extracellular matrix (ECM) gene expression via YAP-TEAD inhibition to evoke spontaneous cell-matrix dissociation and 2) upregulates globin genes to prevent oxidative stress and permit the acquisition of anoikis resistance. Once in the bloodstream, the resulting CTCs could reattach and colonize distant organs to initiate metastatic outgrowth [8]. It remains unclear, however, whether the regulation of CTC anchorage dependency throughout the metastatic cascade requires dynamic plasticity in AST factor expression.

Previously, we observed in mice an induction of AST factors during melanoma CTC dissemination and a subsequent reduction of these factors in colonized lung nodules to levels resembling those of primary tumor cells, suggesting that AST factor expression can show reversible plasticity [4]. In addition, when we triggered a transient induction and reduction of ectopically expressed AST factors, we observed a strong correlation with the loss and gain of

81 anchorage dependency. Although it remains unclear whether these plastic changes in AST
82 expression are important for human cancer metastasis, the direct correlation we observed between
83 AST factor oscillation and the reprogramming of anchorage dependency led us to pursue the
84 hypothesis that the dynamic spatiotemporal modulation of AST factor expression is crucial for the
85 spontaneous dissemination and colonization of CTCs during metastatic outgrowth.

86 Cell-based techniques for studying CTCs, such as suspension cultures in poly-HEMA
87 coated plates or colony-forming assays in soft agar, have focused primarily on investigating the
88 capacity of CTCs to evade anoikis, which is a form of programmed cell death that occurs when
89 cells detach from the ECM [9, 10]. These *in vitro* cell survival assays examine the ability of cancer
90 cells to grow in anchorage-independent conditions and have proven to be one of the most rigorous
91 ways to assess malignancy [11-13]. However, because these assays use trypsinized cells, they
92 cannot mimic the spontaneous process by which CTCs disseminate *in vivo*, nor can they generate
93 the exceedingly rare population of CTC-like cells that can freely detach from adherent culture
94 conditions.

95 To better explore the anchorage plasticity of disseminated cancer cells, we aimed to
96 develop an assay that could comprehensively recapitulate more of the metastatic cascade,
97 beginning with the spontaneous detachment from the primary tumor, the acquisition of anoikis
98 resistance in circulation, and subsequent colonization in distant organs. We therefore developed
99 the dissemination assay, which traces the fate of rare population of CTC-like cells as they undergo
100 dynamic reprogramming of their anchorage plasticity by transitioning between AST and SAT
101 (suspension-to-adherent transition).

102 To investigate adherent-suspension plasticity in cancer patients, we established a
103 comprehensive biobank and analyzed the alteration of AST factor expression during the

104 dissemination and colonization of CTCs. We enrolled untreated *de novo* metastatic breast cancer
105 patients and analyzed single-cell level transcriptomes of matched tissue and liquid biopsy
106 specimens comprising 1) primary tumors, 2) CTCs, and 3) metastatic lesions. To date, most
107 transcriptomic studies in cancer patients seeking to uncover the molecular mechanisms of
108 metastasis have focused on individual analyses of either primary tumors, CTCs, or metastatic
109 lesions. There have also been analyses comparing primary tumors with CTCs or metastatic lesions
110 from unrelated patients [14-18]. To monitor the dynamic plasticity of AST factors and related gene
111 signatures that encompass the metastatic cascade from dissemination to colonization, we have
112 demonstrated the necessity of comparing the transcriptomes of CTCs with the transcriptomes of
113 matched solid tumor counterparts derived from the same patient. Thus, performing a novel cell-
114 based dissemination assay and analyzing single-cell-level transcriptomes of matched specimens
115 from *de novo* metastatic breast cancer patients, our study has revealed how anchorage plasticity
116 drives the metastatic cascade in disseminated CTCs via AST factor-mediated ASP.
117

118 ## Results

119 ### Oscillatory AST factor dynamics regulate anchorage plasticity in cancer cells.

120 Malignant tumors are characterized by the mobilization of cancer cells that have lost
121 contact inhibition of proliferation (CIP). This leads to cell crowding-induced hostile tumor
122 microenvironment (TME) that drives dissemination of CTCs from their primary tumor into the
123 blood vessels, as well as their subsequent colonization of distant sites as metastatic lesions. The
124 metastatic cascade, therefore, could be conceived as a consequence of cancer cells constantly
125 transitioning between the adherent and suspension states.

126 Here, we report a novel cell-based assay termed dissemination assay. Its purpose is to
127 clarify the mechanisms that govern CTC anchorage plasticity (ASP) during the dissemination and
128 colonization processes (**Fig. 1A**). Other *in vitro* cell-based assays widely used in the field, such as
129 suspension culture or colony formation in soft agar, employ trypsinization to artificially detach
130 cancer cells. This procedure 1) bypasses the selection of cells with the ability to self-disseminate
131 and 2) limits the assay to examining the ability to acquire anoikis resistance in trypsinized cancer
132 cells (**Fig. 1B**). The dissemination assay, in contrast, allows for the generation of spontaneously
133 detached CTC-like cells that resemble the natural perturbation of anchorage dependency that takes
134 place in malignant cancer cells as they detach from the primary tumor and reattach at metastatic
135 lesions. Moreover, the dissemination assay allows us to investigate the pathophysiologic cues,
136 cellular plasticity, and molecular mechanisms that regulate the anchorage plasticity of CTCs *in*
137 *vitro*, including the dynamic expression of AST factors in each step.

138 Interestingly, we found that culturing MDA-MB-231 breast cancer cells at high cell
139 density recapitulates the unfavorable and stressful TME that helps drive malignancy, including the
140 nutrient deprivation, acidosis, and mechanical stress. These conditions result in the rounding and
141 detachment of CTC-like cancer cells that resemble the rare population of disseminated CTCs *in*
142 *vivo* (**Fig. 1C**). Notably, we found that these spontaneously detached CTC-like breast cancer cells
143 were then able to acquire anoikis resistance, the capacity for prolonged survival in suspension
144 culture conditions, and the capacity for reattachment and colonization. We next sought to further
145 explore the utility of our dissemination assay to distinguish it from other cell-based assays, such
146 as 1) suspension cultures in poly-HEMA coated plates or 2) colony formation assays in soft agar,
147 which are both commonly used to measure the capacity of malignant cancer cells to evade anoikis
148 in a 3D environment. It is important to note that the most common breast cancer cell lines,

149 including MDA-MB-231, MCF7, BT549, and Hs58T, can survive both suspension culture and the
150 colony formation assay. In contrast, only MDA-MB-231 cells could survive the dissemination
151 assay and produce CTC-like cells. The other breast cancer cell lines we tested exhibited contact
152 inhibition or cell death during the dissemination assay (**Fig. 1D-E**). We hypothesized that the
153 ability of a cell line to produce CTC-like cells in the dissemination assay would likely also reflect
154 its metastatic capacity *in vivo*. To test this, we injected each breast cancer cell line into the fat pad
155 of mice and examined the efficiency with which they disseminated to colonize the lung (**Fig. 1F**).
156 As expected, despite showing similar primary tumor growth, the cell lines that failed to generate
157 CTC-like cells in the dissemination assay showed significantly lower metastatic potential and
158 permitted longer survival than MDA-MB-231 (**Fig. 1G**). This observation correlates with earlier
159 metastasis map (Metmap) findings classifying MDA-MB-231 as one of the most malignant breast
160 cancer cell lines (**Fig. S1A**) [19]. Thus, our *in vitro* dissemination assay permits only the most
161 malignant breast cancer cells to produce spontaneously suspended CTC-like cells.

162 Next, we asked whether CTC-like cells derived *in vitro* through the dissemination assay
163 and *in vivo* CTCs exhibit similar characteristics. We were surprised to find that CTC-like cells
164 recapitulated the aberrant induction of endogenous AST factors, which were highly elevated in
165 CTCs derived from mouse models and *de novo* metastatic breast cancer patients. Detached CTC-
166 like MDA-MB-231 cells expressed much higher levels of the AST factors IKZF1, IRF8, and NFE2
167 than their adhesive counterparts that mirrored the primary tumor (**Fig. 1H**). Notably and in contrast
168 to the CTC-like cells isolated from the dissemination assay, we found significantly lower levels of
169 these AST factors in cells harvested from suspension culture assay (**Fig. S1B**). To verify whether
170 the induction of AST factors is required for the spontaneous detachment of CTC-like cells, we
171 used siRNA to knockdown each factor and measured the dissemination efficiency as an indication

172 of the viability of CTC-like cells produced by the dissemination assay. Although we previously
173 showed that the overexpression of a combination of hematopoietic factors enhanced AST
174 efficiency [4], these knockdown experiments indicated that the depletion of any single AST factor
175 was sufficient to markedly suppress the formation of CTC-like cells (**Fig. 1I**). Moreover, we found
176 that pretreatment with thalidomide derivatives like lenalidomide or pomalidomide, which we
177 previously identified as potential anti-metastatic agents that act by reducing the expression of
178 IKZF1 in mouse breast cancer models [4], substantially inhibited the production of CTC-like cells
179 (**Fig. 1J**). These results demonstrate that AST factor induction is required for the detachment and
180 survival of CTC-like cells in the dissemination assay.

181 The dissemination assay further allowed us to investigate how the CTC-like cells undergo
182 reattachment. When we isolated and replated the CTC-like cells to examine their anchorage
183 plasticity and AST factor expression upon reattachment, we found that CTC-like cells lost their
184 anchorage independence and readily attached to the culture dish to continue proliferating as
185 adherent cells. We refer to these newly adherent cells as met-like cells because they seem to
186 simulate the final stage of the metastatic cascade in which suspended tumor cells in the circulation
187 regain adhesive properties to reattach and colonize a secondary organ. Surprisingly, we found that
188 the met-like cells showed a significant reduction in the increased AST factor expression that had
189 promoted their spontaneous detachment as CTC-like cells, having undergone the suspension-to-
190 adherent transition (SAT) (**Fig. 1K**). These results show that AST factor dynamics in CTC-like
191 cells undergoing AST and SAT transition correlate with the anchorage plasticity of solid tumor
192 cells in a way that is quite distinct from the primary-like or met-like cells. Moreover, because our
193 results establish AST factors as mechanosensitive transcription factors, the mechanisms
194 underlying their mechanical regulation in solid tumor cells warrant further investigation.

195 Proceeding from our previous results establishing the role of AST factor induction in CTC
196 dissemination, we next asked whether AST factor repression is critical for the reattachment and
197 colonization of CTCs *in vivo*. We next generated LM2-AST cells from MDA-MB-231 breast
198 cancer cells selected for its their ability to metastasize to the lung (**Fig. 1L**) [20]. In contrast to
199 control cells, LM2-AST cells stably expressing AST factors elicited spontaneous detachment and
200 anoikis resistance. To determine whether the constitutive activation of AST factors in CTCs
201 impedes lung colonization, we injected LM2-control and LM2-AST cells into the tail vein of
202 NOD/SCID gamma (NSG) mice (**Fig. 1M**). Remarkably, while the LM2-control cells produced
203 successful lung metastases, the stable expression of AST factors in LM2-AST cells dramatically
204 suppressed lung colonization and prolonged survival (**Fig. 1N-P**). This indicates that, while the
205 induction of AST factors evokes CTC dissemination, the subsequent repression of AST factors in
206 CTCs is required for colonization. Together, dissemination assay demonstrates that AST factor
207 dynamics-their induction during the primary-to-CTC transition and their repression during the
208 CTC-to-mets transition-are critical for the dissemination and colonization of CTCs (**Fig. 1Q-R**).
209

210 Adherent-suspension plasticity in the metastatic cascade of *de novo* metastatic 211 breast cancer patients

212 We speculated that ASP is a biologically significant process involved in dynamically
213 regulating the anchorage dependency of CTCs during metastasis *in vivo*. To validate the results
214 obtained from dissemination assay and assess the clinical relevance of ASP in human subjects, we
215 recruited 10 newly diagnosed *de novo* metastatic breast cancer patients and collected matched
216 samples consisting of breast primary tumors, blood cells, and metastatic lesions from each patient
217 (**Table S1**, **Fig. 2A**). Thus, our patient data provides one of the most comprehensive biobanks

218 available to date by analyzing both tissue and liquid biopsy specimens compared to previous
219 studies [14-17]. We then used high density microporous (HDM) chips to enrich CTCs from whole
220 blood via size exclusion. Isolated tissue cells and CTCs were then further processed for single-cell
221 RNA sequencing (scRNA-seq) [21]. We identified epithelial cells, mesenchymal stem cells,
222 fibroblasts, and various immune cells, such as myeloid cells and lymphocytes (**Fig. S2A-B**).
223 Within the overall cell population, we identified cancer cells as those co-expressing EPCAM with
224 the breast cancer-specific cytokeratins KRT5, KRT8, KRT9, KRT17, or KRT18 (**Fig. 2B-C**, **S2A-**
225 **B**). A UMAP analysis revealed a clustering of the cells based on patient and tissue of origin.
226 Interestingly, there was a mixture of cells in the center region consisted of different patients and
227 tissues, where most CTCs were also located (**Fig.2B**). Surprisingly, this region showed higher
228 expression levels of AST factors, including IKZF1, NFE2, and IRF8 (**Fig. 2B**). Upon further
229 examination, we found that the expression of AST factors in CTCs greatly exceeded that of either
230 primary or metastatic tumor cells, with the levels of IKZF1 and IRF8 rising above the statistical
231 significance threshold (**Fig. 2C**, **Fig. S2C**). The increase in AST factor expression was consistent
232 regardless of breast cancer subtype or organ tropism of metastatic tumors. These results
233 demonstrate the clinical relevance of ASP in the metastatic cascade of human patients by
234 regulating the anchorage dependency of CTCs.

235 Previously, when performing a gene set enrichment analysis (GSEA) comparing primary
236 tumors and CTCs, we found significant enrichment of gene sets related to focal adhesion and ECM
237 organization [4]. We confirmed the upregulation of focal adhesion-related genes in both primary
238 tumors and metastatic lesions compared to CTCs (**Fig. S2D**) and the enrichment of ECM
239 organization pathways in metastatic tumors compared to CTCs (**Fig. S2D**). In contrast, CTCs
240 showed a significant decrease in genes related to ECM components and integrins, and a significant

241 increase in the hemoglobin genes HBA1 and HBA2, which protect CTCs against reactive oxygen
242 species (ROS)-induced anoikis (**Fig. 2D**) [4]. These findings in metastatic cancer patients
243 demonstrate that oscillatory AST factor dynamics lead to anchorage plasticity by altering gene
244 expression associated with integrin/ECM components and anoikis resistance.

245 Next, we analyzed the characteristics of CTCs in comparison to their solid tumor
246 counterparts. We focused on the central region of the UMAP, located at similar points in
247 pseudotime analysis (**Fig. 2E**). Cells located outside the central region of the UMAP were
248 clustered together based on cancer stage, tissue origin, and patient identity. The cancer cells were
249 divided into 25 clusters based on gene expression (**Fig. 2E**). To enrich for CTCs in the central
250 region, we considered the following factors: 1) increasing the number of CTCs and 2) enhancing
251 transcript expression similarity among cells, as indicated by a decreased standard deviation of their
252 respective UMAP1 and UMAP2 values (**Fig. S3A-B**). Based on these criteria, we chose eight
253 clusters (i.e., clusters 9, 11, 12, 13, 15, 17, 20, and 24) to represent the center region of the UMAP
254 (**Fig. 2E-F, Fig. S3A**). The center region contains 8,823 solid tumor cells, comprising 3,695
255 primary tumor cells and 5,128 metastatic cancer cells, along with 34 CTCs (**Fig. 2F**). We then
256 examined AST factor expression in cells located within the central region. Pseudotime analysis of
257 the central region clusters indicates a significant increase in AST factor expression, including
258 IKZF1 and IRF8, compared to earlier stages that then decreased again in later stages (**Fig. 2G**).
259 These observations suggest that the transcriptional profile of solid tumor cells from primary and
260 metastatic lesions in the central region resembles that of CTCs, indicating an intermediate state,
261 not yet fully transformed into CTCs [9].

262 To further explore the molecular differences between CTCs and solid tumor cells, as well
263 as the mechanisms underlying the transition observed in the central region, we compared the

264 differentially expressed genes (DEGs) between the two cell types within this region (**Fig**. **2H,**
265 **S3C**), identifying 1,223 CTC-specific and 59 solid tumor-specific genes (**Fig. 2H**). By performing
266 a gene ontology (GO) analysis of the CTC-specific genes, we noticed enrichment of a gene set
267 related to rRNA processing, suggesting ribosome biogenesis is necessary for the protein synthesis
268 that facilitates CTC survival and metastatic potential (**Fig**. **2I**). Although not all superoxide
269 resistance pathways were enriched in the GO analysis, the CTCs in the central region showed
270 specific upregulation of hemoglobin gene, HBA1, which plays an antioxidant role and provides
271 cells with resistance to anoikis, enhancing their metastatic potential (**Fig**. **2J**). In contrast, GO
272 analysis of the solid tumor-specific genes revealed enrichment for terms related to cell adhesion
273 and ECM production (**Fig**. **2I**). These results highlight the distinct cellular behavior of CTCs and
274 solid tumor cells. While CTCs tend to exhibit dynamic, non-adherent properties essential for the
275 survival in circulation, solid tumor cells maintain strong adhesion to the ECM.

276 Psuedotime analysis provided further insights into this transition by revealing that while
277 most solid tumor cells did not express AST factors (AST-negative cells), some positioned at
278 pseudotime points similar to CTCs did exhibit AST factor expression (AST-positive cells) (**Fig**.
279 **2E-F**). To further investigate the differences between these AST-positive and AST-negative solid
280 tumor cells, we conducted DEG analyses comparing the corresponding primary and metastatic
281 tumors. This allowed us to identify 2,112 AST-positive-specific genes and 166 AST-negative-
282 specific genes in the primary tumors versus 1,284 AST-positive-specific genes and 213 AST-
283 negative-specific genes in the metastatic tumors (**Fig**. **2K**). Underscoring the similarity of the two
284 conditions, we found a considerable overlap of 997 AST-positive-specific genes and 45 AST-
285 negative-specific genes that were shared between the primary and metastatic tumors. A GO
286 analysis of these AST-positive-specific genes revealed enrichment in the MAPK- ERK1/2 cascade,

287 which is associated with antioxidant expression, anoikis resistance, and metalloproteinase-
288 mediated ECM degradation (**Fig**. **2L**) [22-25]. In the AST-positive cells, we also identified genes
289 related to extravasation, which suggests that, like CTCs, these cells possess increased invasive
290 properties. In contrast, GO analysis of the AST-negative-specific genes revealed enrichment in
291 pathways related to anchoring junctions, ECM, and focal adhesions, which promote cell adhesion
292 and structural integrity (**Fig**. **2L**). GSEA analysis confirmed that AST-negative cells in both
293 primary and metastatic tumors showed significant enrichment in gene sets related to tight junctions
294 and ECM organization (**Fig**. **2M**). This further supports the notion that AST-negative cells are
295 characterized by strong adhesion properties. In contrast, AST-positive cells, particularly in the
296 central region, co-expressed genes involved in the MAPK cascade, ERK1/2 cascade, and
297 extravasation. Thus, some solid tumor cells exhibit an expression pattern like that of CTCs,
298 indicating the presence of cells with CTC-like characteristics within the solid tumor population.

299 Finally, we analyzed RNA velocity to clarify the correlation of AST factor expression
300 dynamics with the expression of integrin/ECM-related, antioxidant-related, and EMT-related
301 genes (**Fig. 2F, S3D**). Although we found no correlation between AST factors and EMT-related
302 genes, there was a correlation between EMT-related genes and ECM-related genes, which
303 correlates with our previous study that AST is independent of EMT.

304

305 ## Discussion

306 The progression and spread of cancer depend on the cellular mechanisms that enable cancer
307 cells to disseminate from the primary tumor, survive in the circulatory system as CTCs, and
308 establish secondary tumors at distant sites. This complex metastatic cascade is governed by a

309 multitude of biological processes, among which adherent-suspension plasticity (ASP) has emerged
310 as a crucial determinant.

311 Our research highlights that ASP, regulated by the dynamic oscillation of AST factors,
312 plays a fundamental role in facilitating the metastatic spread of breast cancer cells. The plasticity
313 of AST factor expression during metastasis allows cancer cells to shift between adherent and
314 suspension states, enabling them to detach from the primary tumor, survive in the bloodstream,
315 and eventually reattach and colonize secondary sites. The reversible nature of ASP adds a dynamic
316 layer to the metastatic process, suggesting that the transition between adherent and suspension
317 states is not merely a binary switch but rather a finely tuned continuum influenced by intrinsic
318 reprogramming factors.

319 We developed a cell-based experiment termed dissemination assay that simulates how
320 CTCs could achieve spontaneous detachment, anoikis resistance, and reattachment during their
321 journey through the bloodstream. This assay allowed us to elucidate the role of AST factors during
322 the transition of solid tumor cells into CTC-like cells and validate our findings with patient-derived
323 CTCs from individuals with *de novo* metastatic breast cancer. The results confirmed the pivotal
324 role of AST factors in spontaneous CTC dissemination both *in vitro* and *in vivo*. We also
325 demonstrated that, while AST factors facilitate the initial detachment and anoikis resistance of
326 CTCs, their downregulation is essential for the reattachment and successful colonization of cancer
327 cells at distant metastatic sites. This indicates that metastatic success depends on the ability of
328 cancer cells to adapt their anchorage dependency to each stage of metastasis. Suspension
329 characteristics mobilize CTCs into the bloodstream, whereas reattachment and colony formation
330 necessitate a reversion to adherent traits within the microenvironment of secondary sites. These
331 insights challenge the conventional understanding of metastasis as a linear progression and instead

332 propose a model in which anchorage plasticity plays a central role in cancer cells to spread during
333 metastasis. ASP thus represents a novel cellular plasticity mechanism analogous to epithelial-
334 mesenchymal plasticity (EMP), another well-established process that facilitates metastasis,
335 however, limited to the transition between two different adhesive cell types. How cancer cells
336 orchestrate ASP and EMP during each stage of the metastatic cascade warrants further
337 investigation.

338 Our findings underscore the pivotal role of ASP in the metastatic cascade, as demonstrated
339 by scRNA-seq analysis of paired samples from *de novo* metastatic breast cancer patients,
340 encompassing matched primary tumors, CTCs, and metastatic lesions. This dataset offers
341 invaluable insights into tumor progression, adaptability, and heterogeneity across metastatic stages
342 in individual patients. The aggregation of CTCs from different patients within the central region
343 of the UMAP signifies that CTCs exhibit similar transcriptomic profiles despite their origin.
344 Importantly, the significant expression of AST factors not only in CTCs but also in their
345 intermediate solid tumor counterparts from pseudotime analysis indicate that anchorage plasticity
346 from AST to SAT is an adaptive and continuous process throughout the metastatic cascade. The
347 consistency of these trends across tumor subtypes and metastatic locations underscores the broad
348 significance of AST factors as theragnostic biomarkers of metastasis. To elucidate the role of
349 tumor microenvironment as an upstream mediator of AST factors, the spatiotemporal expression
350 patterns of AST factors using matched longitudinal specimens warrants further investigation.

351 Our study provides the rationale for clinical implementation of therapeutic strategies that
352 target AST factors and related mechanisms. For example, therapies designed to inhibit the
353 transition from adherent-to-suspension states, referred to as anti-disseminating agents, could
354 potentially be used as neoadjuvant therapies or alone to impede the initial detachment of cancer

355 cells from the primary tumor, thereby reducing the number of CTCs and the likelihood of
356 metastatic spread. Conversely, strategies that prevent the reattachment of CTCs at secondary sites
357 could hinder metastatic colonization, offering a two-pronged approach to tackle metastasis.
358 Furthermore, our dissemination assay provides a novel platform for screening potential anti-
359 metastatic agents. Traditional assays often fail to capture the full spectrum of phenotypic
360 transitions that occur during metastasis, focusing instead on static endpoints such as cell
361 proliferation or invasion. In contrast, our assay dynamically assesses the ability of cancer cells to
362 undergo adhesive transition, offering a more comprehensive evaluation of their metastatic
363 potential and the efficacy of therapeutic interventions. A deeper exploration into the genetic and
364 epigenetic regulation of AST factors could yield additional mechanistic insights into ASP.
365 Understanding how AST factors are modulated during different stages of metastasis, and the
366 interplay between ASP and other forms of cellular plasticity, such as EMP, warrants further
367 investigation to delineate how these processes collectively contribute to the completion of
368 metastasis.

369 Together, our findings highlight the unprecedented role of ASP in breast cancer metastasis.
370 ASP provides a novel theoretical basis in cancer metastasis and suggests AST factors as promising
371 therapeutic targets to tackle the metastatic spread of solid tumor cells. Clinically, moving beyond
372 the primary tumor-centric point-of-view, our data expand the prevailing cancer treatment paradigm
373 toward direct intervention within the metastatic processes. The availability of cell-based platforms
374 that measure ASP efficiency and multi-omics database of matched longitudinal patient samples
375 could facilitate future research opportunities, including individualized metastasis prediction
376 models, hence augmenting the potential for developing effective anti-metastatic therapies [26].
377

Conclusion

Our results demonstrate that ASP mediated by the plasticity of AST factors is critical for the metastatic dissemination and colonization of solid tumor-derived CTCs. Using a novel dissemination assay and single-cell transcriptomic analyses of matched metastatic breast cancer patient specimens, we elucidate the dynamic plasticity of AST factor expression in solid tumor cells that promotes the transition between adherent and suspension states, enabling CTCs to detach, resist aniokis, and reattach at distant metastatic sites. These findings highlight the potential of targeting AST factors to develop effective anti-metastatic therapies.

Abbreviation

AST : Adherent-to-Suspension Transition

SAT : Suspension-to-Adherent Transition

ASP : Adherent-Suspension Plasticity

Mets : Metastases

CTCs : circulating tumor cells

LEN : Lenalidomide

POM: Pomalidomide

t-SNE : t-stochastic neighbor embedding

UMAP : Uniform Manifold Approximation and Projection

NSG : NOD/SCID gamma

399 DEGs : differentially expressed genes

400 PCA : Principal components analysis

401 nTPM : normalized transcripts per kilobase million

402 GO : Gene Ontology

403 UMIs : unique molecular identifiers

Declarations

Ethical approval

Ethical approval for the use of human subjects was obtained from the Institutional Review Board of Gangnam Severance Hospital, Yonsei University, Seoul, Republic of Korea (3-2021-0236) in compliance with the ethical guidelines of the 1975 Declaration of Helsinki, and informed written consent was obtained from each patient. Collection of human breast cancer samples were obtained from consenting patients in accordance with guidelines and regulations approved by the Institutional Review Board of Gangnam Severance Hospital, Yonsei University Health System (3-2021-0236). The animal experiment protocols were reviewed and approved by the Yonsei University Institutional Animal Care and Use Committee (IACUC).

Competing interests

The authors declare that they have no conflict of interest.

Fundings and acknowledgments

This work was supported by grants from the National Research Foundation of Korea (2020M3F7A1094077, 2020M3F7A1094089, 2021R1A2C1010828, RS-2024-00509461, to H.W.P., 2018R1A5A2025079, 2020M3F7A1094091 to H.Y.G.), by Global - Learning & Academic research institution for Master's·PhD students, and Postdocs (LAMP) Program of the National Research Foundation of Korea grant funded by the Ministry of Education (RS-2024-00442483 to H.W.P.), by the Brain Korea 21 FOUR Program (to H.D.H., Y.S., H.L., B.J.H., W.Y.P., J.O., and D.K.L.)

427 ## Authors' contributions

428 H.D.H., Y.S., and J.H.K. performed most of the experiments. H.L., B.J.H., W.Y.P. performed drug
429 treatment and imaging. J.O., and D.K.L. performed transcriptome analyses. H.-C.L., S.P., and J.C.
430 performed CTC isolation and scRNA-seq. Y.S.C. performed experiments regarding matrix
431 stiffness and cell imaging. J.J., H.Y.G., and H.W.P. designed the study and wrote the manuscript.

432

433 ## Data and material availability

434 All single cell RNA sequencing data are deposited in the Korean Nucleotide Archive (KoNA,
435 https://www.kobic.re.kr/kona/) and the Korean BioData Station (KBDS,
436 https://www.kobic.re.kr/kbds/). The KoNA data is deposited under project ID KAP220346, and
437 the KBDS data is deposited under project ID KAP240986.

438

439 ## References

440 1. Chaffer CL, Weinberg RA: A perspective on cancer cell metastasis. *Science* 2011,
441 331:1559-1564.
442 2. Nguyen DX, Bos PD, Massague J: Metastasis: from dissemination to organ-specific
443 colonization. *Nat Rev Cancer* 2009, 9:274-284.
444 3. Marabitti V, Caruana I, Nazio F: Should I stay or should I go? Spatio-temporal control of
445 cellular anchorage by hematopoietic factors orchestrates tumor metastatic cascade. *Mol*
446 *Cancer* 2023, 22:149.
447 4. Huh HD, Sub Y, Oh J, Kim YE, Lee JY, Kim HR, Lee S, Lee H, Pak S, Amos SE, et al:
448 Reprogramming anchorage dependency by adherent-to-suspension transition promotes
449 metastatic dissemination. *Mol Cancer* 2023, 22:63.
450 5. Huh HD, Park HW: Emerging paradigms in cancer cell plasticity. *BMB Rep* 2024, 57:273-
451 280.
452 6. Lee JY, Huh HD, Lee DK, Park SY, Shin JE, Gee HY, Park HW: Reprogramming
453 anchorage dependency to develop cell lines for recombinant protein expression. *Biotechnol*
454 *J* 2024, 19:e2400104.
455 7. Smit DJ, Hoffer K, Bettin B, Kriegs M, Cayrefourcq L, Schumacher U, Pantel K, Alix-
456 Panabieres C, Jucker M: Analysis of the Plasticity of Circulating Tumor Cells Reveals
457 Differentially Regulated Kinases During the Suspension-to-Adherent Transition. *Cancer*
458 *Med* 2024, 13:e70339.
459 8. Massague J, Obenauf AC: Metastatic colonization by circulating tumour cells. *Nature*
460 2016, 529:298-306.

461 9. Lee DK, Oh J, Park HW, Gee HY: Anchorage Dependence and Cancer Metastasis. *J*
462 *Korean Med Sci* 2024, 39:e156.
463 10. Weiswald LB, Bellet D, Dangles-Marie V: Spherical cancer models in tumor biology.
464 *Neoplasia* 2015, 17:1-15.
465 11. Puck TT, Marcus PI, Cieciura SJ: Clonal growth of mammalian cells in vitro; growth
466 characteristics of colonies from single HeLa cells with and without a feeder layer. *J Exp*
467 *Med* 1956, 103:273-283.
468 12. Borowicz S, Van Scoyk M, Avasarala S, Karuppusamy Rathinam MK, Tauler J, Bikkavilli
469 RK, Winn RA: The soft agar colony formation assay. *J Vis Exp* 2014:e51998.
470 13. Woods NT, Yamaguchi H, Lee FY, Bhalla KN, Wang HG: Anoikis, initiated by Mcl-1
471 degradation and Bim induction, is deregulated during oncogenesis. *Cancer Res* 2007,
472 67:10744-10752.
473 14. Koch C, Kuske A, Joosse SA, Yigit G, Sflomos G, Thaler S, Smit DJ, Werner S, Borgmann
474 K, Gartner S, et al: Characterization of circulating breast cancer cells with tumorigenic and
475 metastatic capacity. *EMBO Mol Med* 2020, 12:e11908.
476 15. Sun YF, Wu L, Liu SP, Jiang MM, Hu B, Zhou KQ, Guo W, Xu Y, Zhong Y, Zhou XR,
477 et al: Dissecting spatial heterogeneity and the immune-evasion mechanism of CTCs by
478 single-cell RNA-seq in hepatocellular carcinoma. *Nat Commun* 2021, 12:4091.
479 16. Ebright RY, Lee S, Wittner BS, Niederhoffer KL, Nicholson BT, Bardia A, Truesdell S,
480 Wiley DF, Wesley B, Li S, et al: Deregulation of ribosomal protein expression and
481 translation promotes breast cancer metastasis. *Science* 2020, 367:1468-1473.
482 17. Garcia-Recio S, Hinoue T, Wheeler GL, Kelly BJ, Garrido-Castro AC, Pascual T, De
483 Cubas AA, Xia Y, Felsheim BM, McClure MB, et al: Multiomics in primary and metastatic

484 breast tumors from the AURORA US network finds microenvironment and epigenetic
485 drivers of metastasis. *Nat Cancer* 2023, 4:128-147.
486 18. Turajlic S, Xu H, Litchfield K, Rowan A, Chambers T, Lopez JI, Nicol D, O'Brien T,
487 Larkin J, Horswell S, et al: Tracking Cancer Evolution Reveals Constrained Routes to
488 Metastases: TRACERx Renal. *Cell* 2018, 173:581-594 e512.
489 19. Jin X, Demere Z, Nair K, Ali A, Ferraro GB, Natoli T, Deik A, Petronio L, Tang AA, Zhu
490 C, et al: A metastasis map of human cancer cell lines. *Nature* 2020, 588:331-336.
491 20. Minn AJ, Gupta GP, Siegel PM, Bos PD, Shu W, Giri DD, Viale A, Olshen AB, Gerald
492 WL, Massague J: Genes that mediate breast cancer metastasis to lung. *Nature* 2005,
493 436:518-524.
494 21. Lee SJ, Lee CH, Choi SH, Ahn SH, Son BH, Lee JW, Yu JH, Kwon NJ, Lee WC, Yang
495 KS, et al: Evaluation of a novel approach to circulating tumor cell isolation for cancer gene
496 panel analysis in patients with breast cancer. *Oncol Lett* 2017, 13:3025-3031.
497 22. Li F, Liang H, You H, Xiao J, Xia H, Chen X, Huang M, Cheng Z, Yang C, Liu W, et al:
498 Targeting HECTD3-IKKα axis inhibits inflammation-related metastasis. *Signal Transduct*
499 *Target Ther* 2022, 7:264.
500 23. Yuan S, Norgard RJ, Stanger BZ: Cellular Plasticity in Cancer. *Cancer Discov* 2019,
501 9:837-851.
502 24. Fanelli GN, Naccarato AG, Scatena C: Recent Advances in Cancer Plasticity: Cellular
503 Mechanisms, Surveillance Strategies, and Therapeutic Optimization. *Front Oncol* 2020,
504 10:569.

505 25. Akhmetkaliyev A, Alibrahim N, Shafiee D, Tulchinsky E: EMT/MET plasticity in cancer
506 and Go-or-Grow decisions in quiescence: the two sides of the same coin? *Mol Cancer*
507 2023, 22:90.
508 26. Anderson RL, Balasas T, Callaghan J, Coombes RC, Evans J, Hall JA, Kinrade S, Jones
509 D, Jones PS, Jones R, et al: A framework for the development of effective anti-metastatic
510 agents. *Nat Rev Clin Oncol* 2019, 16:185-204.
511 27. Shin JE, Kim SH, Kong M, Kim HR, Yoon S, Kee KM, Kim JA, Kim DH, Park SY, Park
512 JH, et al: Targeting FLT3-TAZ signaling to suppress drug resistance in blast phase chronic
513 myeloid leukemia. *Mol Cancer* 2023, 22:177.
514

Figure 1. AST plasticity in the novel *in vitro* dissemination assay.

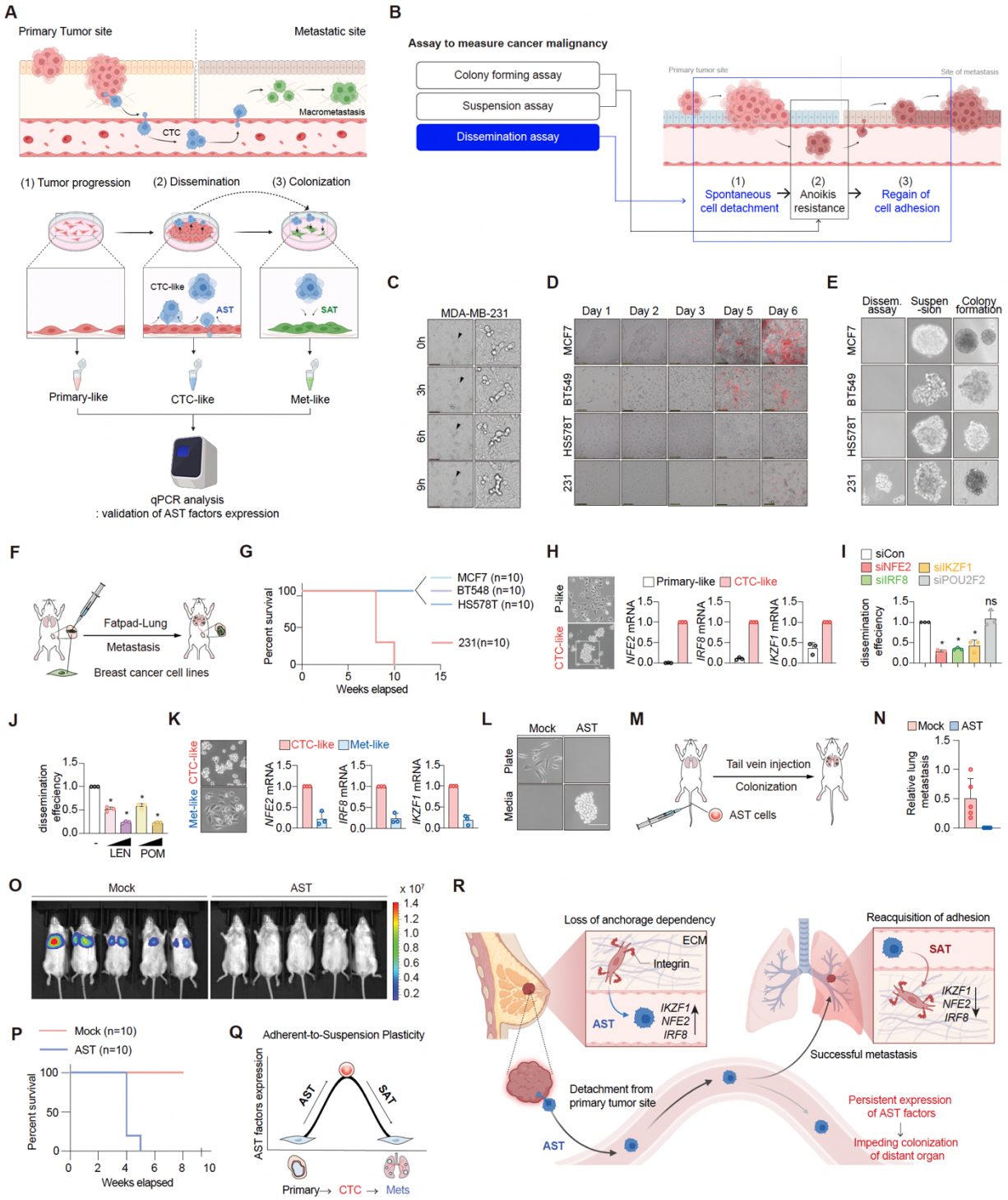

519 **Figure 1. AST plasticity in the novel *in vitro* dissemination assay.**

520 **A**, Schematic overview of the dissemination assay. **B**, Schematic overview of 3 different assays
521 for cancer malignancy and the steps of the metastatic cascade they address. **C**, Time-lapse
522 microscopy images showing spontaneous cell detachment of MDA-MB-231 cells in the
523 dissemination assay. **D**, Representative fluorescence images MCF7, BT549, Hs578T and MDA-
524 MB-231 cells stained for viability with propidium iodide. Red, dead. Scale bars, 100 μm. **E**,
525 Representative images of MCF7, BT549, Hs578T and MDA-MB-231 cell morphology in the
526 indicated assay conditions. **F**, Schematic overview of mammary fat pad xenografts of 4 different
527 breast cancer cell lines. **G**, Kaplan-Meier survival plot showing the survival rates of mice injected
528 with MCF7, BT549, Hs578T, or MDA-MB-231 cells. **H**, Representative images of suspended
529 MDA-MB-231 cell morphology in the dissemination assay and quantitative real-time PCR
530 analysis of AST factor transcript levels in CTC-like cells. **I**, Dissemination efficiency for MDA-
531 MB-231 cells following siRNA-mediated AST factor depletion. N = 3. **J**, Dissemination efficiency
532 for MDA-MB-231 cells following treatment with lenalidomide or pomalidomide. N = 3. **K**,
533 Representative images of re-attached MDA-MB-231 cell morphology in the dissemination assay
534 and quantitative real-time PCR analysis of AST factor transcript levels in met-like cells compared
535 to CTC-like cells. **L**, Representative images of LM2-mock or 3AST cell (LM2 cells expressing
536 AST factors) morphology on a culture plate or in media. **M**, Schematic overview of tail vein
537 injections with 3AST cells. **N**, Bioluminescence images of lung metastases after LM2 tail vein
538 injections. **O**, Lung metastases quantified by lung bioluminescence intensity for mock versus
539 3AST cells. **P**, Kaplan-Meier survival plot showing the survival rates of mice injected with mock
540 or 3AST cells. N = 10. **Q, R**, Schematic illustrating mechanistic insights and significance of AST
541 plasticity in the context of the metastatic cascade.

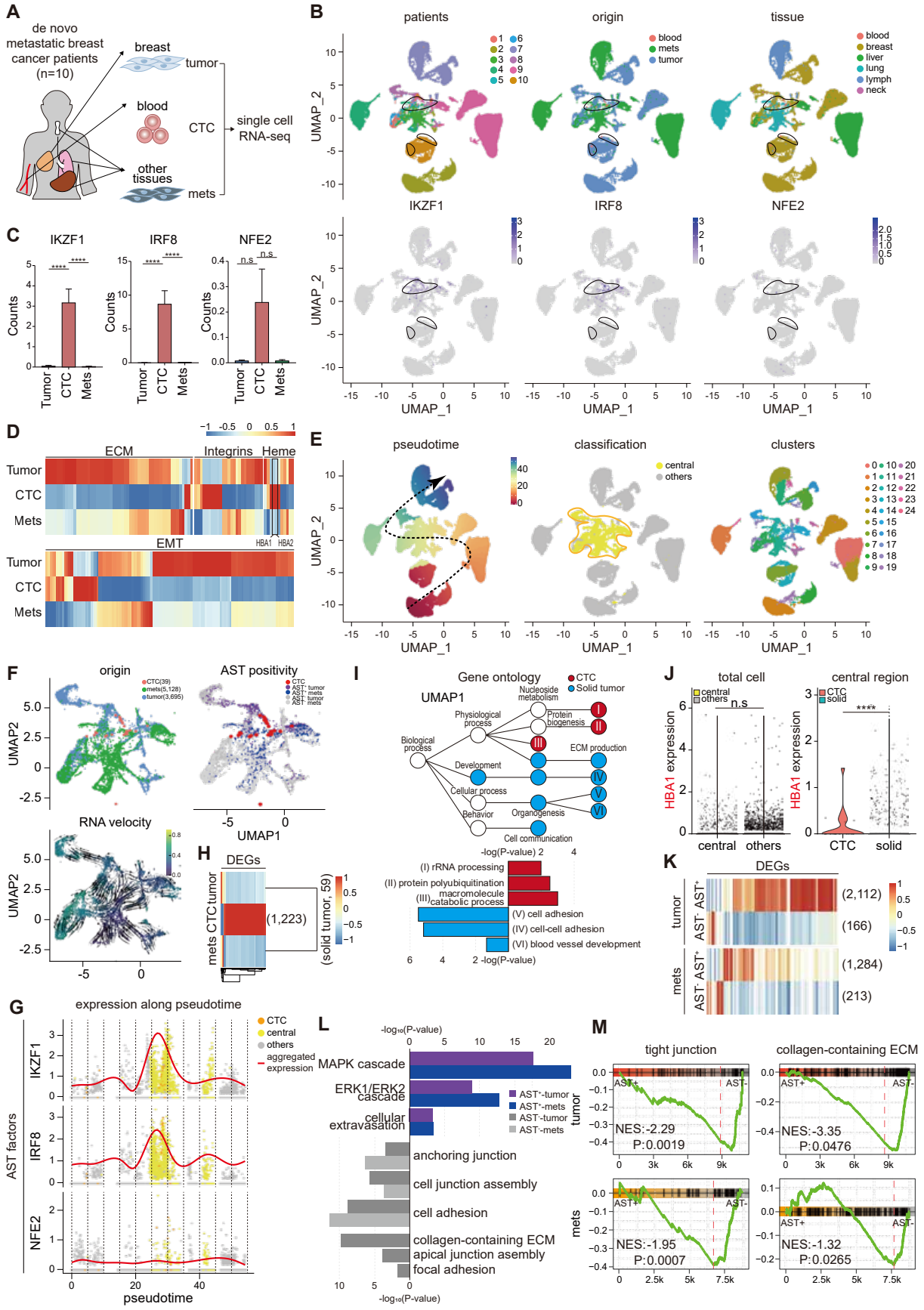
A
de novo metastatic breast cancer patients (n=10)
breast
tumor
blood
CTC
other tissues
mets
single cell RNA-seq
B
patients
origin
tissue
blood
mets
tumor
blood
breast
liver
lung
lymph
neck
UMAP_2
UMAP_1
IKZF1
IRF8
NFE2
C
IKZF1
IRF8
NFE2
Counts
Tumor
CTC
Mets
n.s
D
ECM
Integrins
Heme
Tumor
CTC
Mets
EMT
HBA1
HBA2
E
pseudotime
classification
clusters
central
others
F
origin
AST positivity
UMAP2
UMAP1
RNA velocity
H
DEGs
mets CTC tumor
(1,223)
(solid tumor, 59)
I
Gene ontology
CTC
Solid tumor
UMAP1
Nucleoside metabolism
Physiological process
Protein biogenesis
Biological process
ECM production
Development
Cellular process
Organogenesis
Behavior
Cell communication
-log(P-value)
(I) rRNA processing
(II) protein polyubiquitination
(III) macromolecule catabolic process
(V) cell adhesion
(IV) cell-cell adhesion
(VI) blood vessel development
J
total cell
central region
central
others
n.s
HBA1 expression
CTC
solid
K
DEGs
tumor
mets
AST+
AST-
(2,112)
(166)
(1,284)
(213)
G
expression along pseudotime
CTC
central
others
aggregated expression
AST factors
IKZF1
IRF8
NFE2
pseudotime
L
-log10(P-value)
MAPK cascade
ERK1/ERK2 cascade
cellular extravasation
AST+-tumor
AST+-mets
AST-tumor
AST-mets
anchoring junction
cell junction assembly
cell adhesion
collagen-containing ECM
apical junction assembly
focal adhesion
M
tight junction
collagen-containing ECM
tumor
mets
NES:-2.29
P:0.0019
NES:-3.35
P:0.0476
NES:-1.95
P:0.0007
NES:-1.32
P:0.0265

542

543 **Figure 2. AST plasticity in matched single cell RNA-seq samples from *de novo* breast**
544 **cancer patients.**

545 **A,** Schematic overview of the isolation and scRNA-seq analysis of primary tumor cells,
546 circulating tumor cells (CTCs), and metastatic tumor cells from de novo metastatic breast cancer
547 patients (n = 10). CTCs were isolated using HDM chips. **B**, Uniform manifold approximation
548 and projection (UMAP) of scRNA-seq cells (n = 10; 54,866 cells) colored by patient, origin,
549 tissue, and normalized gene expression of the AST factors IKZF1, IRF8, and NFE2. Black
550 border lines, area in which the CTCs are located. **C**, Dynamite plots showing the expression of
551 (left) IKZF1, (middle) IRF8, and (right) NFE2 in primary tumor cells, CTCs, and metastatic
552 tumor cells. ****, $P < 0.0001$; n.s, not significant ($P > 0.05$). **D**, Heatmaps showing normalized
553 expression of four gene sets—ECM, integrins, antioxidant defense genes, and EMT-related
554 genes—in primary tumors, CTCs, and metastases. The average normalized expression values for
555 cells within each group are displayed as scaled values. Black-bordered box, HBA1 and HBA2.
556 **E**, UMAP plot showing (left) pseudotime, (middle) a division between the central region
557 containing complex clusters with CTCs and others, and (right) clusters calculated at a resolution
558 of 0.5. Dotted arrow, flow of pseudotime for the normalized gene expression of the AST factors
559 IKZF1, IRF8, and NFE2. **F**, UMAP of the central region colored according to origin, AST
560 positivity, and RNA velocity. **G**, Pseudotime expression plots showing AST factors. X-axis,
561 pseudotime; y-axis, expression levels; gray dots, others; yellow dots, central region; orange dots,
562 CTCs; red line, linear expression trend using generalized additive modeling (GAM). **H**, Heatmap
563 showing differentially expressed genes (DEGs). DEGs were identified based on comparisons
564 between solid tumor cells and CTCs within the central region and selected with a threshold p-
565 value < 0.05. There were 1,223 CTC DEGs and 59 solid tumor DEGs. **I**, Gene ontology tree
566 showing the CTC-specific gene set and the solid tumor-specific gene set with a bar plot showing

567 the gene names and the p-values corresponding to the circles marked with roman numerals.
568 Colored circles, statistically significant, FDR corrected $P < 0.01$. **J**, Violin plots with dots
569 showing HBA1 expression. The first plot compares the central region with other groups, while
570 the second plot compares CTCs with solid tumor cells within the central region. Yellow, central
571 region; gray, others; orange, CTCs within the central region; turquoise, solid tumor cells within
572 the central region; ****, $P < 0.0001$; n.s, not significant ($P > 0.05$). **K**, Heatmap showing DEGs.
573 In a comparison of cells with and without AST factor expression in both primary and metastatic
574 tumors, the DEG thresholds were defined as an FDR corrected q-value < 0.001 and an absolute
575 fold change > 2. **L**, Bar plot showing ontology analysis results for the AST-positive and AST-
576 negative gene sets identified in (**K**). Purple bars, AST-positive gene sets in primary tumors; blue
577 bars, AST-positive gene sets in metastatic tumors; gray bars, AST-negative gene sets in primary
578 tumors; light gray bars, AST-negative gene sets in metastatic tumors. **M**, Gene set enrichment
579 analysis (GSEA) results for tight junction and collagen-containing ECM gene sets within both
580 primary and metastatic tumors.

581 **Supplementary Figure 1. The dissemination assay is distinct from other assays, such as**

582 **the colony formation or suspension assays.**

583

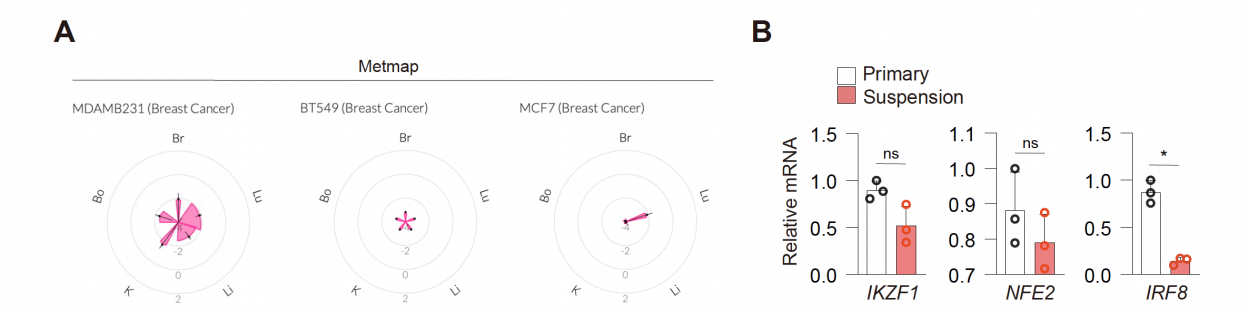

584

585

586 **A**, Petal plots showing the metastatic patterns of 3 breast cancer cell lines. Data for these plots

587 were obtained from Jin, X., *et al*. (https://depmap.org/metmap). **B**, Quantitative real-time PCR

588 analysis of AST factor transcript levels in cells harvested from suspension assay.

Supplementary Figure 2. Comprehensive overview of single cell RNA sequencing data from breast cancer patients.

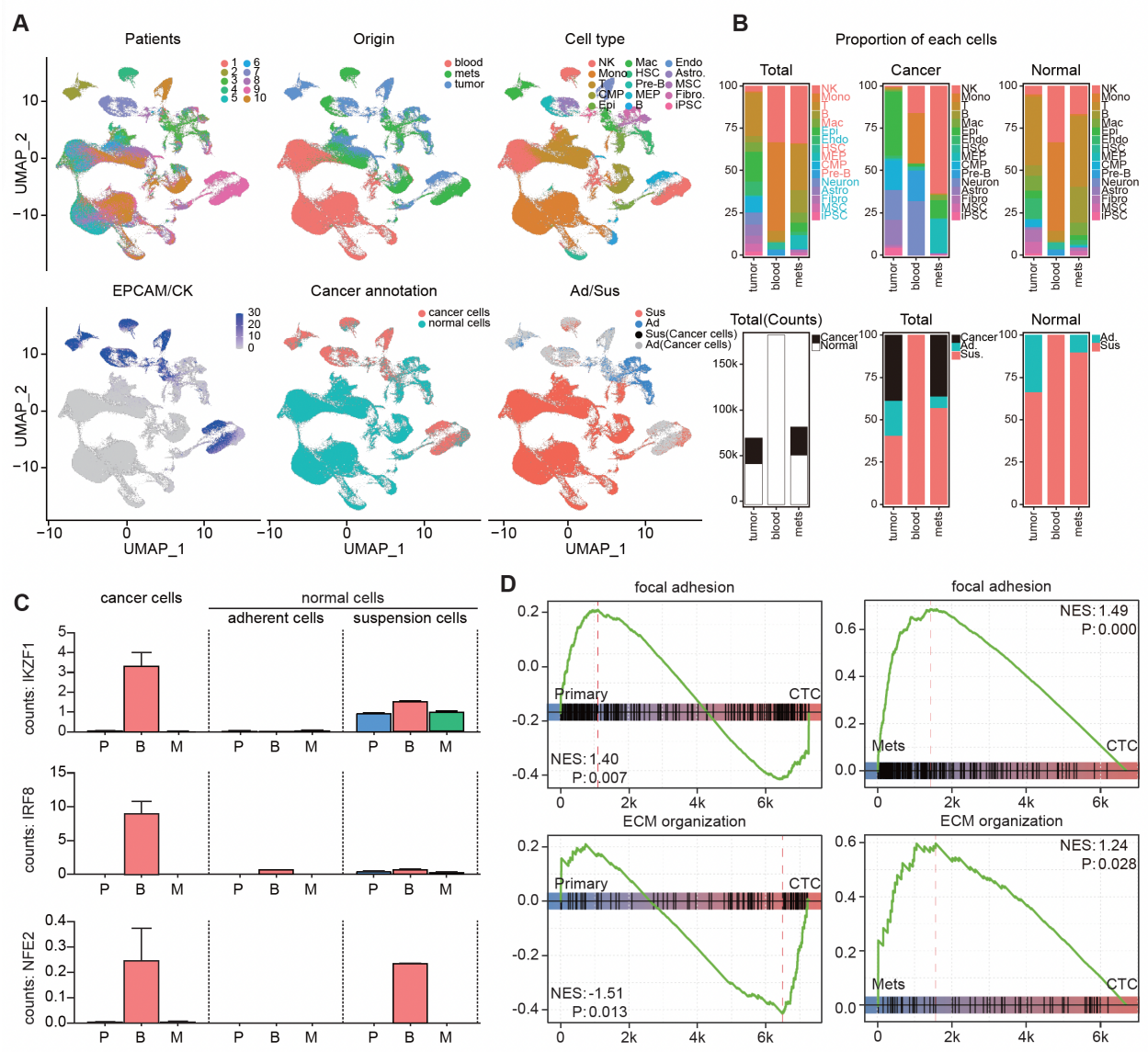

A, Uniform manifold approximation and projection (UMAP) of scRNA-seq cells (n = 316,539 cells) colored by patient, origin, cell type, normalized gene expression of cancer cell markers (EPCAM, KRT5, KRT7, KRT8, KRT18, and KRT19), cancer/non-cancer annotation, and the combined cancer/non-cancer and adherent/suspension annotation. **B**, Bar plots showing a breakdown of cell type composition across tumor, blood, and metastasis samples. The first row

597 shows the proportion of various cell types in total cells, cancer cells, and normal cells. The
598 second row shows the proportion of cancer cells versus normal cells, adherent versus suspension
599 cells within cancer and normal cells, and adherent versus suspension cells within normal cells. **C**,
600 Dynamite plots depicting the expression of the AST factors IKZF1, IRF8, and NFE2 in cancer
601 cells from primary tumor, blood, and metastases, as well as normal cells split into adherent and
602 suspension states. **D**, Gene set enrichment analysis (GSEA) plots for focal adhesion and ECM
603 organization gene sets comparing CTCs to primary tumor or metastatic cells.

604 **Supplementary Figure 3. Central region-specific cell populations and CTC–solid tumor**

605 **divergence in scRNA sequencing data.**

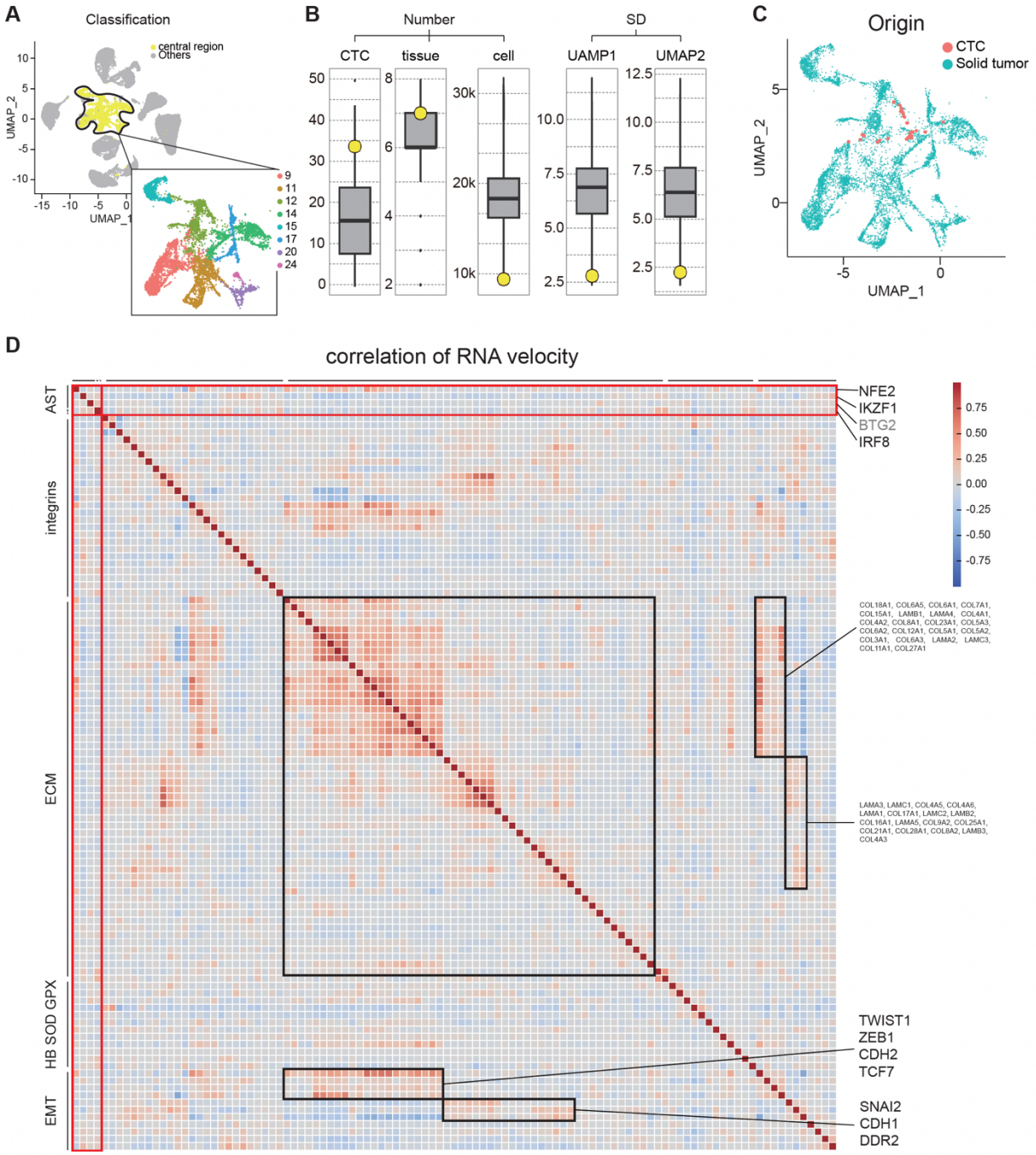

606

607

608 **A**, UMAP of cancer cells categorized into the central region and others. A magnified view of the
609 central region is also shown to highlight its specific clusters. **B**, Boxplots of 1,081,575 cluster
610 combinations (binomial coefficient with n = 25, k-permutation = 8) presenting numbers of CTCs,
611 originating tissues, and total cells with standard deviations (SDs) for UMAP1 and UMAP2. Yellow
612 dot, selected cluster combination; CTCs, n = 34, 11.93%; originating tissues, n = 7, 8.83%; total
613 cells, n = 8,857, 99.31%; UMAP1 SD, 2.77, 90.69%; UMAP2 SD, 2.49, 0.36%. **C**, UMAP of cells
614 in the central region colored by anchorage status. Turquoise, solid tumor; orange, CTCs. **D**,
615 Heatmap of RNA velocity correlations among AST factor, ECM, integrin, superoxide resistance
616 genes, and EMT genes.

617 **Table S1. Overview of patient information used for single cell transcriptome analysis.**

Patient #	Metastasis tissue	Subtype	Total cell counts			Cancer cell counts		
			Tumor	Blood	Meta	Tumor	Blood	Meta
patient1	liver	Her2	1,746	7,209	2,411	659	2	1,033
patient2	neck	Luminal-B	13,246	9,499	-	9,198	-	-
patient3	lung	Her2	14,254	25,180	11,982	516	1	2,531
patient4	lung	Luminal-B	-	25,394	10,900	-	2	7,507
patient5	brain	Her2	1,569	19,071	-	82	1	-
patient6	lung	TNBC	3,612	13,166	5,034	324	1	19
patient7	lymph	Luminal-A	9,572	26,768	9,404	4,438	8	5,833
patient8	neck	TNBC	11,741	9,117	12,746	1,257	7	13
patient9	liver	Luminal-A	8,077	21,471	16,458	5,032	9	11,641
patient10	lymph	TNBC	5,795	14,629	10,138	4,721	19	13
			69,612	171,504	79,073	26,227	50	28,590

618

619 **Movie S1. Dissemination assay of various breast cancer cell lines**

620 **A**, Video of MCF7 cell proliferation in the dissemination assay.

621 **B**, Video of BT549 cell proliferation in the dissemination assay.

622 **C**, Video of HS578T cell proliferation in the dissemination assay.

623 **D**, Video of MDA-MB-231 cell proliferation in the dissemination assay.

624 # METHODS

625 ## DNA constructs

626 AST genes were tagged with V5 and subcloned into the pENTR4 vector (Addgene, 17425 and
627 17423) using standard molecular cloning techniques. The resulting subcloned vectors were then
628 recombined with the destination vector pLentiCMV (Addgene, 17293) using LR recombinase
629 (Invitrogen, 1179019), generating the final lentiviral expression vectors.

630

631 ## Cell culture

632 Cells were maintained in a 37 °C humidified incubator with 5% CO_2. HEK293T, MCF7, HS578T
633 and MDA-MB-231 cells were cultured in DMEM (Hyclone, SH30022.01). BT549 cells were
634 cultured in RPMI (Hyclone, SH30027.01). Culture media were supplemented with 10% FBS
635 (Hyclone, SV30207.02) and 1% penicillin/streptomycin (Invitrogen, 15140122).

636

637 ## Dissemination assay

638 Dissemination assays were performed using MDA-MB-231, MCF7, BT549, and HS578T cells,
639 with each cell line cultured in its own respective growth media. For the assay, the cells were seeded
640 on normal plates at 80% confluency on the first day and then maintained for 3 days without any
641 media changes. After 3 days, the cells surpass 100% confluency, resulting in very high cell density.
642 After the old media were replaced with fresh media, the cells were cultured for an additional 3
643 days at 100% confluency. We noticed MDA-MB-231 cells began to round up and detach from the
644 plate beginning on the second day after the media change. By the third day, we observed a higher
645 number of CTC-like cells. These detached CTC-like cells were harvested by collecting the media,
646 followed by centrifugation to isolate the cells. For MCF7 cells, despite the media change, the cells

647 began to die after 3 days. Although BT549 and HS578T cells did not exhibit cell death, they did
648 cease proliferating.
649
650 **Viral infection**
651 Viral infection was performed as previously described [27]. To generate lentiviral particles,
652 HEK293T cells were transfected with plasmids encoding pMD2G and psPAX2, along with the
653 lentiviral vectors containing the desired constructs. Transfections were performed using Polyplus
654 Reagent (Merck) according to the manufacturer's protocol. At 48 hours post-transfection, media
655 containing the viral particles were harvested from the transfected cells. The harvested media were
656 then filtered through a 0.45 µm filter to remove cellular debris. To enhance infection efficiency,
657 the filtered media were supplemented with 8 mg/ml polybrene. The transduced cells were infected
658 with the lentiviral particles by incubating them with the filtered media. After 24 hours of infection,
659 the media were changed, and the cells were incubated for another 24 hours. Then, transduced cells
660 were selected using puromycin. The selection process allowed for the enrichment of cells that
661 successfully integrated the lentiviral vectors and expressed the desired genes or markers.
662
663 **Cell viability assay**
664 *In vitro* cell viability was assessed using the CellTiter Glo® 2.0 cell viability assay (Promega,
665 G9241) and the LIVE/DEAD® cell imaging kit (ThermoFisher, R37601) according to their
666 manufacturers' protocols. For the suspension assay, cells were plated on Corning® Costar® Ultra-
667 Low Attachment Multiple-Well Plates (Merck, CLS3471).
668
669 **Quantitative real-time PCR analysis**

670 Cellular RNA samples were collected via RNA extraction using the RNeasy Plus mini kit
671 (QIAGEN, 74136). These RNA samples were then reverse transcribed into complementary DNA
672 (cDNA) using iScript reverse transcriptase (Bio-Rad, 1708891). The KAPA SYBR FAST qPCR
673 kit (Kapa Biosystems, KK4605) and the 7300 real-time PCR system (Applied Biosystems) were
674 used for quantitative real-time PCR (qRT-PCR). The following primer sequences were used for
675 qPCR: IKZF1, 5'-TTTCAGGGAAGGAAAGCCCC-3' (forward) and 5'-
676 CTCCGCACATTCTTCCCCAT-3' (reverse); NFE2, 5'-ACAGCTGTCCACTTCAGAGC-3'
677 (forward) and 5'-TGAGCAGGGGCAGTAAGTTG-3' (reverse); IRF8, 5'-
678 AGCATGTTCCGGATCCCTTG-3' (forward) and 5'-CGGTCCGTCACTTCCTCAAA-3'
679 (reverse); and ACTB, 5'-GCCGACAGGATGCAGAAGGAGATCA-3'(forward) and 5'-
680 AAGCATTTGCGGTGGACGATGGA-3'(reverse).
681

682 **siRNA transfection**

683 A transfection mix was prepared by combining 100 µl of Opti-MEM™ medium (ThermoFisher,
684 #31985070), 12 µl of RNAi Max transfection reagent (Invitrogen, 13778150), and 2 µl of 20 µM
685 siRNA. The following siRNAs were used for transfection: non-silencing (NS) siRNA (Dharmacon
686 siGENOME non-targeting control pool #D-001206-13-200), siIKZF1 (Dharmacon siGENOME
687 SMARTPool #M-019092-01-0010), siNFE2 (Dharmacon siGENOME SMARTPool #M-010049-
688 00-0010), siIRF8 (Dharmacon siGENOME SMARTPool #M-011699-01-0010), and siPOU2F2
689 (Dharmacon siGENOME SMARTPool #M-019690-01-0010).
690

691 **Mouse model experiments**

692 All animal experiment protocols in this study underwent a thorough review and received approval
693 from the Yonsei University Institutional Animal Care and Use Committee (IACUC). All

694 procedures involving animals adhered to the Guidelines for the Care and Use of Laboratory
695 Animals. The NOD SCID Gamma (NSG) mice used for orthotopic injection experiments were
696 obtained from JA Bio. For the orthotopic mouse model experiments, mammary fat pads of 7-week-
697 old female NSG mice were orthotopically injected with $1x10^6$ MCF7, BT549, HS578T, or MDA-
698 MB-231 cells. For the mouse tail vein injection experiments, the tail veins of 7-week-old female
699 NSG mice were injected with $1x10^5$ MDA-MB-231 derivative LM2 cells. At week 4, the mice
700 were euthanized for bioluminescence imaging using the In Vivo Imaging Spectrum (IVIS) device
701 (PerkinElmer, CLS136331 IVIS Lumina LT Inst, Series III, 120 V). All *in vivo* experiments were
702 carried out using mice that had received the same treatment. The NSG mice used in these
703 experiments possessed an identical genotype and genetic background.
704

705 **Statistical analyses**

706 All quantitative data were obtained from at least three independent biological replicates. Data are
707 presented as means ± standard deviation (SD) unless otherwise noted in the figure legends.
708 Statistical differences between two groups were examined using two-tailed, unpaired Student's t-
709 tests or one-way analysis of variance (ANOVA) with Bonferroni corrections for multiple
710 comparisons. Statistical tests were performed using the GraphPad Prism 9.0 software (GraphPad
711 Software, CA, USA). Two-sided p-values of less than 0.05 were considered significant. No
712 statistical methods were used to predetermine sample size. Sample size was based on previous
713 experience with experimental variability. Blinding was performed wherever possible during all
714 sample analysis by coding sample identity during data collection and having the analysis
715 performed by an observer without knowledge of or access to the experimental conditions.
716

717 **Bioinformatics of primary tumor cells, CTCs, and metastatic cancer cells**

718 The illumina outputs for human samples were mapped to the human reference genome (GRCh38)
719 using Cell Ranger 7.1.0 (10X Genomics). Gene-wise read counts for genes with at least 500 reads
720 were exported from Cell Ranger to the Matrix Market format and imported into R with Seurat's
721 Read10X function. An average of > 135 million reads from > 13,000 cells were obtained for each
722 sample. Each 10X library was individually checked for quality, and the cells were filtered
723 according to the same criteria used in our previous study to ensure good gene coverage [4]. After
724 quality control filtering, a total of 310,189 cells remained, with 69,612 cells from the primary
725 tumor site, 171,504 cells from the blood, and 79,073 cells from the metastatic site (**Table 1**).
726 Samples were combined via an algorithm implemented in Seurat. The default Seurat function
727 settings were used, and 1:20 principal component dimensions were used for all dimension
728 reduction and integration steps. The cluster resolutions were set to 0.5, unless otherwise stated.
729 The RunUMAP random seed was set to 1,000 to ensure reproducibility. Marker genes for cell
730 clusters were identified using Seurat's FindMarkers function with the default settings. Cell type
731 annotation was performed using the SingleR package (v2.6.0) with the HumanProteinAtlas
732 database from the celldex package (v1.14.0). Cells co-expressing EPCAM and cytokeratins such
733 as KRT5, KRT8, KRT9, KRT17, or KRT18 were designated as cancer cells. A total of 54,867
734 cells were used for the analysis, including 26,227 cells from the primary tumor site, 50 cells from
735 the blood, and 28,590 cells from metastatic sites (**Table 1**). The cells designated as cancer cells
736 were subsequently extracted and reanalyzed beginning with the normalization process. DEGs were
737 selected with thresholds for the FDR corrected p-value < 0.001 and an absolute $\log_2$ fold change
738 ≥ 1. GO analysis was performed using the gseGO function from clusterProfiler (v3.0.4). GSEA
739 plots were generated from the DEG data using the gseaplot function. Pseudotime analysis was
740 performed using the monocle package (v3.0) with normalized data, UMAP coordinates, and cluster

741 information obtained from the initial Seurat analysis. The calculation of gene set scores along
742 pseudotime was conducted for each cell using the AddModuleScore function in Seurat. All plots
743 were exported to the PDF format using R and their dimensions were adjusted in Illustrator.